Mem. S.A.It. Vol. 95, 22

Memorie della

The Integral Field Imager and Spectrometers for Planetary Exploration ($\int$ISPEx)

G. Filacchione[1], M. Ciarniello[1], M. Tarabini[2], E. Mazzotta Epifani[3], C. Cencia[1], B. Saggin[2], G. Piccioni[1], A. Raponi[1], I. Di Varano[1], Z. Kanuchova,[3,4], P. Palumbo[1], I. Guerri[4], A. Taiti[4], I. Ficai Veltroni[4], M. Barilli[4], and S. Pelli[5]

[1] Istituto Nazionale di Astrofisica (INAF) – Istituto di Astrofisica e Planetologia Spaziali (IAPS), Via del Fosso del Cavaliere 100, I-00133 Roma, Italy e-mail: gianrico.filacchione@inaf.it
[2] Politecnico di Milano, Polo Territoriale di Lecco, Via G. Previati 1/C, 23900, Lecco, Italy
[3] Istituto Nazionale di Astrofisica (INAF) – Osservatorio Astronomico di Roma (OAR), Via Frascati 33, 00040, Monte Porzio Catone (RM), Italy
[4] Astronomical Institute of the Slovak Academy of Sciences, 059 60 Tatranska Lomnica, The Slovak Republic
[5] Leonardo SpA, Electro-Optical Business Unit, Via A. Einstein, 35, 50013 Campi Bisenzio (FI) – Italy

Received: 26 March 2024; Accepted: 18 May 2024

Abstract. The study of planetary bodies needs high resolution images and reflectance spectra to infer morphology and composition. In this context a new optical concept has been introduced in the $\int$ISPEx (Integral Field Imager and Spectrometers for Planetary Exploration) instrument which integrates a Color Camera and an Integral Field Spectrometer. Thanks to this innovative optical design, it is possible to acquire at the same time color images and reflectance spectra through a single telescope. In this work, we define the configuration of the $\int$ISPEx$_{0.4}^{5.0\mu m}$ space model, which operates in the 0.4-5.0 μm spectral range and we discuss its optical performances, thermomechanical and electronic architecture. The breadboard $\int$ISPEx$_{0.4}^{1.0\mu m}$ operating in the 0.4-1.0 μm spectral range is also presented to demonstrate the overall optical concept. It has been realized using commercial optical components and its spectral and spatial performances have been tested in the IAPS laboratories.

Key words. Instrumentation: visible color camera - visible and infrared imaging spectrometer. Techniques: integral-field spectroscopy

1. Introduction

This study's main objective is to analyze how to merge two imaging spectrometers and a color camera into a single space payload. The resulting instrument concept is the Integral Field Imager and Spectrometers for Planetary Exploration ($\int$ISPEx). In this regard, we are also proposing the introduction of novel op-

tical photonic devices that can increase the functionality of existing cameras and imaging spectrometers. The camera architecture allows for high flexibility in the selection of the bandpass and bandwidth of the color filter in order to be adapted to very different scientific targets. In fact, broad bandpass filters are better suited to observe rocky and icy surfaces, while narrowband filters are preferentially used to observe through atmospheric windows or gaseous emissions. As opposed to conventional whiskbroom and pushbroom instruments, a VIS-IR integral field imaging spectrometer is built to acquire the whole hyperspectral cube in a single acquisition, greatly reducing the acquisition time (Fig. 1). The camera and imaging spectrometer will share comparable observation modes as a result of the methods we are going to describe later, greatly simplifying their operations. The fISPEx will provide an advantage in this regard by enabling a better utilization of the data gathered by the two channels concurrently, which will be quite advantageous for many scientific cases. In fact, using this synergistic approach, it will be feasible to examine high resolution color images to study the interpretation of a target's shape while simultaneously retrieving composition and physical quantities from hyperspectral data. Applying sharpening algorithms to spectrometer images is made possible by the availability of camera images. In addition, an integral-field spectrometer, while maintaining the capabilities of more conventional whiskbroom and pushbroom spectrometers, will outperform them in situations where the target scene is rapidly evolving and viewing conditions change during the acquisition. In fact, traditional instruments are constrained by the possibility that the hyperspectral image ("cube") acquisition process may take more time than the temporal scale during which the investigated event evolves. In this instance, observations are made in order to study the dynamical development of planetary atmospheres, lightning strikes, hypervelocity impacts, or fast-moving objects. An Integral-Field spectrometer can effectively resolve the four dimensions of the scene (two-dimensional spatial, one spectral, and one temporal dimension) by adopting large area and rapid readout detectors, enabling the acquisition of time-resolved hyperspectral movies. The increased operability of Integral-Field spectrometers during fast flyby phases, when the target's distance and illumination geometry are quickly changing and only a small window of time is available to examine the target under ideal conditions, is another significant benefit of these instruments. An Integral-Field spectrometer can attain image capabilities comparable to those of cameras by collecting the whole hyperspectral cube in a fraction of the time required to complete the scan for a conventional scanning spectrometer.

2. Scientific Requirements: a case study

The fISPEx instrument has the flexibility to acquire hyperspectral data in a wide range of conditions, making it appropriate for conducting scientific investigations of planetary surfaces and atmospheres. In this manuscript, we discuss the sensor performances for a typical Near Earth Asteroid (NEA) mission scenario. We have chosen the NEA 2008EV5 as a case study since it has already been investigated within the framework of the NASA's Asteroid Redirect Robotic Mission (ARRM) and the European Space Agency's Marco Polo. This asteroid is also a potential target for the next AEM/Zheng'He sample-return mission from China. Thanks to recent advancements of space technology, we have had the opportunity to achieve a close distance exploration at five Near Earth Asteroids in the past 20 years. The second biggest NEA (433) Eros was orbited by the NASA spacecraft Near Earth Asteroid Rendezvous (NEAR-Shoemaker) in February 2000. This was the first "rendez-vous" mission aiming to a small body. The Japanese spacecraft Hayabusa, the first asteroid sample return mission, reached (25143) Itokawa in 2005 and accomplished its goal by returning a sample of the asteroid's surface to Earth five years later. Chinese unmanned lunar mission Chang'e 2

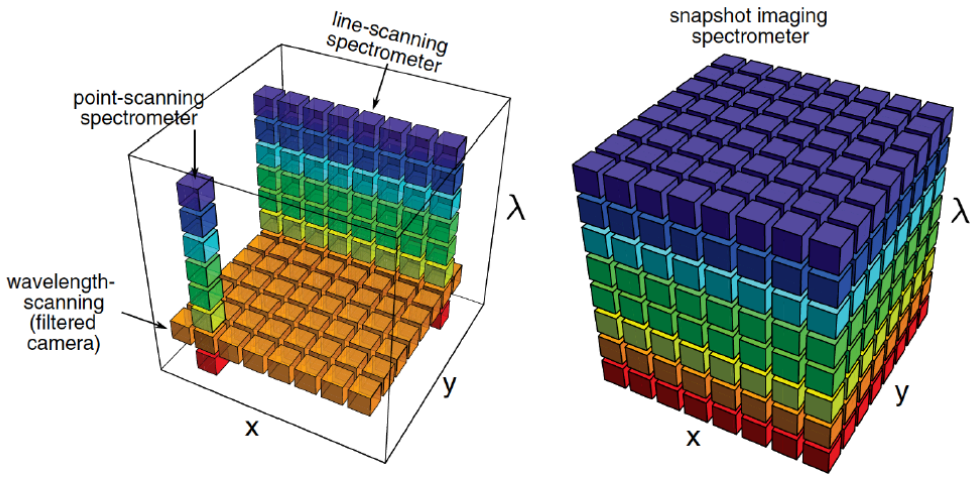

Fig. 1. Possible acquisition modes for an hyperspectral cube. The spatial axes are marked as x, y. The spectral axis by λ. Left panel: time scanning by point (whisk-broom), by line (push-broom), or by wavelength (filter camera). Right panel: single exposure integral field (snapshot) imaging spectroscopy. Figure from (Hagen and Kudenov 2013).

achieved a new milestone in December 2012 when it successfully flew past NEO (4179) Toutatis, passing within 770 meters of the asteroid's surface. Two additional NEOs were visited by dedicated sample return missions in 2018: the Japanese spacecraft Hayabusa2 landed twice on the asteroid Ryugu (162173) in June to gather samples, which will was returned to Earth in December 2020 via a reentry capsule. As a result, the mission was extended; it will now arrive at NEA 1998 KY26 in 2031, following a flyby of NEA 2001 CC21 in 2026. The potentially Earth-impacting asteroid (101955) Bennu was visited by NASA's OSIRIS-REx (Origins, Spectral Interpretation, Resource Identification, and Security-Regolith Explorer) in December 2018. Bennu's surface sample was collected by OSIRIS-Rex in October 2020 after it successfully touched down there. The sample has been returned to Earth on September 24, 2023 and it is currently under investigation. When compared to Earth-based studies, asteroids can be studied with an unmatched degree of accuracy thanks to space missions. We only learned about the small-scale structure of asteroids thanks to the first high-resolution images of the surfaces of Eros and subsequently Itokawa acquired by imagers onboard specialized space missions. Detailed examination of the visited objects yields extremely exact information on their size, shape, mass (and subsequently, density), rotation, and surface characteristics. These parameters are essential for understanding the physics of the object under investigation. Furthermore, whatever the method of mitigation, they are essential to design any future planetary defense space mission. Studies of asteroids that will never be visited by a space mission can reveal the ground truth by com-

paring features of asteroids obtained through space mission observations with ground-based observational results and data-analysis techniques. Framing cameras and spectrometers that operate at visible and/or infrared wavelengths are common remote sensing instruments onboard space missions aiming to investigate Solar System objects: the data returned by these experiments may be used to immediately infer a number of essential properties and comprehensive information on the shape, composition, and physical processes taking place on the targets.

2.1. Scientific requirements for the Imager (IMG)

In order to thoroughly analyze the morphology and topography of the 2008EV5 surface, high spatial resolution images will be required. In addition, high spatial resolution images are essential for characterizing the target body in terms of: 1) topography of the surface and the distribution of features (such as boulders, craters, and fractures); 2) development of a digital elevation model with an accuracy of typically 1 m in height and spatial resolution with respect to the center of mass, in both illuminated and unlit regions; 3) analysis of the history and evolution of NEO fragmentation and accretion; 4) bulk composition of the body (size, shape, rotational properties); and 5) overall characteristics: orbit, rotation, size, shape, mass, gravity and density. High spatial resolution images are necessary for S/C navigation as well as for the investigation of mineralogical and chemical composition (using images taken with a narrow-band filters). The following list represents the Imager (fISPEx-IMG) functional requirements: at least 12 distinct colors spanning the visible spectral range must be acquired on the whole surface of 2008EV5 with a spatial resolution greater than 25 cm/px from a distance of 15 km. The local solar elevation angle must be ranging between 0◦ and 60◦ elevation. Additionally, in order to create global maps across several revolutions, the camera must be able to take full-disk images of the asteroid surface (diameter = 400 m) from a distance of 15 km. At a resolution of 7 cm/px, high quality images taken from a distance of 5 km will capture regions of interest that are about 300 × 150 m wide. The imager must be built to have an average SNR of more than 100 at λ=0.55 μm for observations made at phase angle ϕ = 30°.

2.2. Scientific requirements for the Imaging Spectrometer (SPE)

To acquire a thorough description of the mineralogical composition of the various geologic units (terrains, crater walls and floors, ejecta), an imaging spectrometer is required. Investigation of surface petrology and mineralogy is primarily obtained by visible and near-infrared wavelength spectroscopy. Analysis of spectra characteristics that are indicative of the existence and composition of certain mineral species and other materials predicted on the target body allows one to derive the compositional characterization of asteroids. In their NIR reflectance spectra, the majority of minerals exhibit diagnostic absorption characteristics which allow to identify them. For this reason a moderate (<20 nm) spectral sampling is necessary for the identification of the majority of mineral phases. Organic compounds are expected to be found on most primitive bodies. They need higher spectral sampling (<5 nm) to be detected. For example, for fundamental silicates like olivine and pyroxene it is possible to learn about their chemistry, e. g. the amount of Fe in olivine and the abundance of Ca in pyroxene, measuring their respective 1 and 2 μm band position and band strength ratios which are known for ortophyroxene (low Ca) and clinopyroxene (high Ca). Phyllosilicates, a kind of secondary minerals, can be identified thanks to their diagnostic water and OH absorption bands located at 1.4, 1.9, and in the 2.9-3.3 μm range. Carbonates show other bands in the 2.0-3.3 μm and 3.9-4.0 μm range. Asteroids of the C taxonomic type in particular, which are thought to be connected to carbonaceous chondrites, may display hydrated

silicates on their surfaces, whilst D types are anticipated to be rich in organic compounds. Both aromatic and aliphatic species of organic materials exhibit distinguishing spectral bands in the 3.0-3.7 μm range. The identification of such species requires a spectral sampling <5 nm. The central wavelength and width of the observed mineral bands on asteroids are reported in Table 1.

The imaging spectrometer ($\int$ISPEx-SPE) must be able to acquire hyperspectral data in the spectral range of 0.4-5.0 μm with a spectral sampling better than 5 nm/band for wavelengths $\lambda < 1$ μm and better than 10 nm/band for wavelengths $1 \leq \lambda \leq 5$ μm. The spatial resolution must be better than 3.5 m/px from a distance of 15 km. High resolution data of a region of interest acquired at a spatial scale better than 1.5 m/px shall be acquired from a distance of 5 km. The spectrometer must be able to achieve an average SNR of more than 100 throughout the entire spectrum range for observations made at a phase angle of $phi = 30°$.

2.3. Operational requirements

The scientific requirements discussed in the previous sections are meet by the $\int$ISPEx optical requirements as reported in Table 2.

The fast rotation rate of 2008EV5 (3.725 h) places operational restrictions on the maximum integration of the imager and spectrometers. The dwell time (t_{dwell}), which is the amount of time required to change the projection of one pixel on the surface by one Instantaneous Field-Of-View (IFOV), must be taken into consideration while tuning the integration time. In the hypothesis of a nadir pointing spacecraft orbiting around a spherical body, through the equation

$$t_{dwell} = \frac{IFOV \cdot D}{v_{sub}} \quad (1)$$

where D is the spacecraft's altitude and v_{sub} is the sub-spacecraft point velocity, it is possible to correlate the dwell time with the orbital characteristics of the platform from which observations are carried out. We make the assumption that the maximum integration time will be 0.33 times the dwell duration in order to prevent smearing. The formulation of a specific mission scenario is outside the purview of this study, however for the D=5 and 15 km orbit scenarios, we are supposing a maximum $v_{sub} < 5$ m/s and < 1 m/s, respectively. The imager and spectrometer's maximum dwell times and integration times under these circumstances are listed in Table 3. In order to comply with the maximum integration time while preventing saturation, the optimal integration timings must be chosen.

The asteroid's surface spins at a rate of around 10 cm/s, therefore using the parameters predicted in Table 3, it is not necessary to account for this effect during either the global mapping phase starting at D=15 km or the high resolution phase starting at D=5 km. Since the IMG channel will have integration periods of ≤ 1 s, the predicted smearing caused by the asteroid rotation will be less than the pixel resolution. For more detailed mission scenarios, these values can be assessed more favorably.

3. Instrument description

The $\int$ISPEx instrument employs a single telescope to feed an imager equipped with a liquid crystal tunable filter (LCTF) and two VIS and IR integral field spectrometers using coded mask optical reformatters (CMOR).

The instrument feeds a collimated light beam to the entrance pupils of the camera and spectrometers using a Three Mirror Afocal Telescope with a 2.4X beam reduction factor. The telescope is designed with an input pupil diameter of 84 mm, and an output pupil diameter of 35 mm). A beamsplitter and a dichroic filter are used to align the FOVs of the two channels on a single boresight. In addition to reducing bulk by using a single telescope, this technique enables the camera and imag-

Table 1. Spectral absorption features associated with hydrated minerals on asteroids.

Wavelength (μm)	Width (μm)	Transition	Reference
< 0.4	> 0.1	$Fe^{2+} \rightarrow Fe^{3+}$ intervalence charge	Gaffey and McCord (1979)
0.43	0.02	$6A1 \rightarrow 4A1, 4E(G)$ Fe^{3+} spin-forbidden as in Jarosite	Vilas et al. (1993)
0.60-0.65	0.12	$6A1 \rightarrow 4T2(G)$ Fe^{3+} in Fe alteration minerals	Vilas et al. (1994)
0.70	0.3	$Fe^{2+} \rightarrow Fe^{3+}$ phyllosilicates	Vilas and Gaffey (1989)
0.80-0.90	0.08	$6A1 \rightarrow 4T1(G)$ Fe^{3+} in Fe alteration minerals	Vilas et al. (1994)
3.0	> 0.7	structural hydroxyl (OH) interlayer and adsorbed H_2O	Lebofsky (1978, 1980)
3.07	0.2	H_2O ice NH_4-bearing saponite	Lebofsky et al. (1981) King et al. (1978)

Table 2. Instrumental optical requirements for: imager channel (IMG), visible spectral channel (SPE-VIS) and infrared spectral channel (SPE-IR).

Channel	Requirement	Value
IMG	IFOV	14 μrad
	FOV	3.3° × 1.6°
	Spectral Range	0.42-0.73 μm
SPE-VIS	IFOV	100 μrad
	FOV	0.4°
	Spectral Range	0.4-1.05 μm
	Spectral Sampling	4 nm/band
SPE-IR	IFOV	225 μrad
	FOV	0.28°
	Spectral Range	0.95-5.0 μm
	Spectral Sampling	8 nm/band

ing spectrometer to operate simultaneously, greatly simplifying their operations. The optical bandpass (in the 0.42-0.73 μm spectral range) and associated bandwidth (from 16 nm at 0.42 μm to 48 nm at 0.73 μm) of a liquid crystal tunable filter (LCTF) mounted on the entry pupil of the camera objective can be user-chosen by adjusting the polarization voltage applied to the filter.

In order to achieve a spatial resolution of 0.14 m/px from a distance of 10 km, the camera optical design assures a 3.3° × 1.6° FOV and an IFOV of 14μrad. The integral field imaging spectrometers further split the FOV in two spectral channel: the VIS in the 0.4-1.05 μm spectral range with 3.2 nm/band sampling, and the IR within the 0.95-5.0 μm spectral range with a 8 nm/band sampling. To gather the hyperspectral cube through a single acquisition, these channels employ specially designed Coded Mask Optical Reformatters (CMOR) created from bundles of optical fibers. With respect to spectrometers operating in whiskbroom or pushbroom mode, this creative method allows for a significant reduction in acquisition time. The FOV/IFOV for the VIS and IR spectrometers, respectively, are 0.4° (circular)/100 μrad and 0.28° × 0.28° (square)/225 μrad. The VIS spectrometer constructs a circular hyperspectral picture of 70 m in diameter from a distance of 10 km, using 4000 pixels with a 1 m/px resolution; at the same 10 km distance, the IR spectrometer builds a 50×50 m image made of 22×22 pixels with a resolution of 2.25 m/px. Finally, the 3.3° × 1.6° FOV and the 14μrad IFOV allow the the camera optical design to attain a spatial resolution of 0.14 m/px from a distance of 10 km.

$\int$ISPEx will provide an edge in this regard by enabling better utilization of the data gathered by the three channels, which will be extremely advantageous for many scientific projects. By using a synergistic approach, it will be feasible to use high-resolution images to limit how a target's morphology is inter-

Table 3. Instrumental dwell time and maximum integration time for mapping from altitude D=15 km and high resolution observations from D=5 km. Times are computed for sub-spacecraft velocity of v_{sub} < 1 m/s and < 5 m/s, respectively.

	D=15 km			D=5 km		
Channel	$t_{dwell}(s)$	res(m/px)	$t_{exp}(s)$	$t_{dwell}(s)$	res(m/px)	$t_{exp}(s)$
IMG	0.21	0.21	0.07	0.014	0.07	0.005
SPE-VIS	1.5	1.5	0.5	0.1	0.5	0.03
SPE-IR	3.4	3.4	1.1	0.22	1.1	0.07

preted while retrieving composition and physical attributes from hyperspectral data that was simultaneously acquired. Spectrometers' images may be improved using sharpening algorithms because camera images are readily available. This applies to investigations looking at the dynamical development of planetary atmospheres, lightning strikes, cometary outbursts, hypervelocity impacts, or any fast-moving objects. An integral Field spectrometer can effectively resolve the four dimensions of a given dataset (2D spatial, spectral, and temporal) by functioning with rapid readout detectors, providing the opportunity to create time-resolved hyperspectral movies. Integral Field spectrometers also have improved operability during fast flyby phases, when the target's distance and illumination geometry change quickly and there are only a few windows of opportunity for the target to be seen under ideal conditions. An Integral Field spectrometer may achieve a degree of imaging flexibility comparable to that of a camera by collecting the full hyperspectral cube in a fraction of the time required to finish the scan for a typical scanning spectrometer.

Here, we present the best solution currently in use for the flying configuration that adheres to the plan given in Fig. 2. The adopted configuration was chosen to satisfy the following requirements: 1) To maximize the radiometric performance of the instrument, the LCFT filter with the largest clear aperture possible (O=35 mm) was used. As a result, the LCTF spectral response (0.42-0.73 μm) determines the IMAGER channel's spectral range; 2) the focal length and f/# of the IMAGER objective are determined by the imager channel's FOV and other scientific needs, as well as the detector of choice (pixel size). The IMAGER detector's pixel size was chosen to restrict the objective's focal length (and thus, the volume of this subsystem); 3) The f/#, core size, and fISPEx requirements (IFOV) of the optical fibers have been used to define the parameters of the VIS and IR objectives; 4) The length of the terminal B of the fiber bundles and the core sizes of the optical fibers have been used to define the slit dimensions of the spectrometers. 5) The pixel size of the spectrometers' detectors has been chosen as a trade off between the detectors model available on the market and the resulting magnification of the spectrometers channel (a unitary magnification is preferred); 6) The design of the spectrometer was influenced by the required spectral range and resolution, slit length, manufacturing/alignment viability, and volume/mass reduction. The resulting instrument design is described in detail in the following sections based on these drivers.

3.1. Optical Head (OH)

A shared telescope that feeds the Imager and Spectrometer channels through a beam splitter and a dichroic filter is part of the Optical Head (OH). The two spectrometers are depicted in the right panel of Figure (3), while the depiction of the fISPEx telescope and imager is presented in the left panel. A 50/50 beam splitter (4) divides the collimated optical beam leaving the telescope (labeled 1, 2, and 3 in Fig. 3), with one half of the flux being reflected into the imager channel through a folding mirror (5) to minimize OH volume. Before the beam reaches the imager's focusing objective (7) and detector, the LCTF (6) filters it in

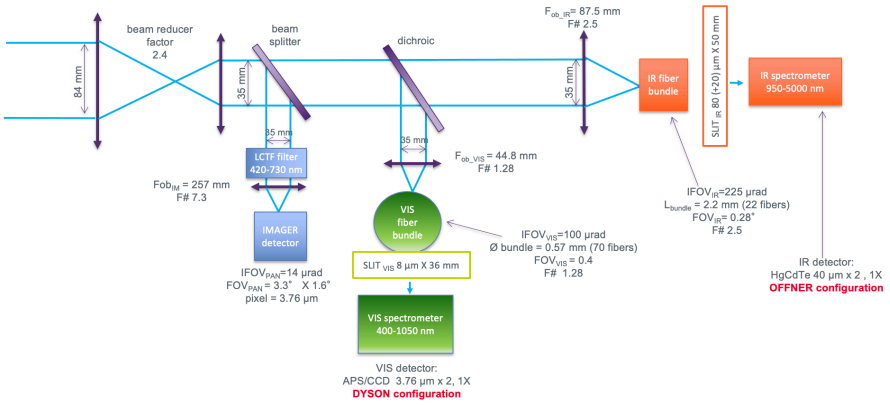

Fig. 2. Instrument optical design summary. In blue the Imager channel, in green the VIS spectrometer, and in orange the IR specctrometer.

wavelength between 420 and 730 nm (8). The second half is transmitted to the two spectral channels through a dichroic filter (9), which reflects visible wavelengths ($\lambda \leq 1$ μm) towards the SPE-VIS channel focusing objective (10), while transmitting infrared wavelengths ($\lambda \geq 1$ μm) on the SPE-IR channel focusing objective (12) after reflection on a folding mirror (11). By maintaining a collimated beam of 35 mm diameter at the entry pupil of each of their objectives, this approach enables the separation of the three optical beams toward the imager and spectrometers in their respective spectral regions.

3.2. The Three Mirror Afocal (TMAf) telescope

The ƒISPEx telescope is based on a three mirrors unobstructed afocal design (TMAf), with an circular aperture pupil of 84 mm and a 35 mm output aperture pupil (beam reduction factor x2.4). The telescope's field of view (FOV) is ±0.6875° along the X axis and ±0.333° along the Y axis. Thanks to the previously indicated reduction factor, this design allows to match the imager FOV. The out-of-field straylight will be rejected with the aid of an internal baffle positioned in proximity of the intermediate field stop situated between M2 and M3. The mirrors are designed to receive a silver coating to maximize their reflectance. With this configuration the predicted transmission and polarization sensitivity of the TMAf telescope as a function of wavelength, on the axis field, and on the maximum FOV along both directions (already qualified for space applications by Leonardo Company) has been simulated. According to the optical study, the largest distortion occurs along the X and Y axes at ±0.3% and ±0.04%, respectively, while the transmission is consistently greater than 85%, with a mean value of 92%.

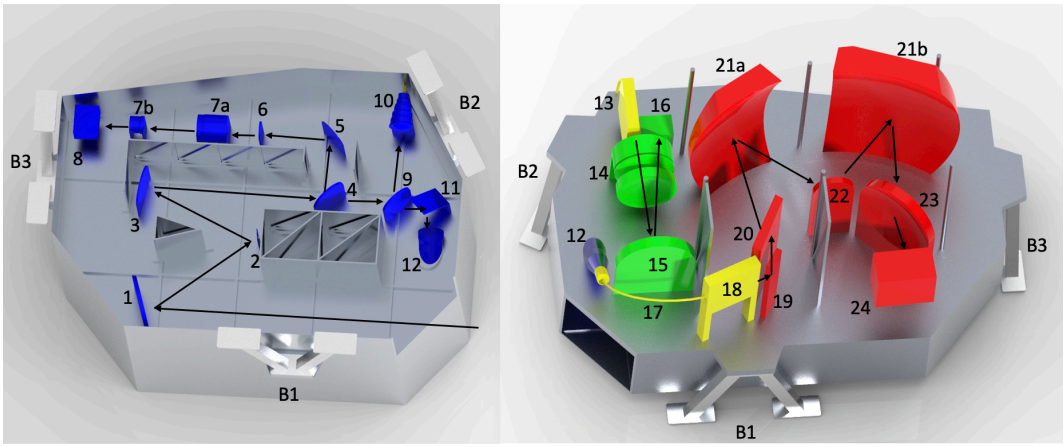

Fig. 3. Optical and mechanical layout. Telescope and Imager side optical bench (left panel): Off-Axis Afocal Telescope primary (1), secondary (2) and tertiary (3) mirrors, beam splitter (4), imager feed folding mirror (5), LCTF (6), imager objective (two groups of lenses, 7a-7b), imager detector (8), dichroic filter (9), VIS spectrometer objective (10), folding mirror (11), IR spectrometer objective (12), bipods (B1-B2-B3). Spectrometers' side optical bench (right panel): IR spectrometer objective (12), VIS optical fibers bundle and CMOR equivalent slit (13), VIS Dyson spectrometer lenses (14), VIS concave grating (15), VIS detector (16), IR optical fibers bundle (17), IR CMOR and equivalent slit (18), folding mirror (19), corrective lens (20), IR Offner spectrometer primary mirror caps (21a-21b), IR grating (22), corrective lens (23), IR detector (24).

3.3. Imager (IMG) optical layout

Liquid Crystal Tunable Filter (LCTF) Using a Liquid Crystal Tunable Filter (LCTF), the Imager captures color pictures in the spectral region of 0.42-0.73 μm. By using polarizers, the filter alters the polarization of light when transmitted through birefringent optical components; this assembly is referred to as a "stage" of the filter. A stage's first polarizer offers a predetermined input polarization. Depending on the light's wavelength, birefringent wave plates, also known as retarders, alter the polarization of the light to varying degrees. The light of some polarizations is then attenuated by the exit polarizer, thereby blocking light at undesirable wavelengths. By altering the value of each retarding element, birefringent filters may be tuned. By adjusting the voltage applied to the stages, nematic liquid crystals, employed as solid state electro-optic retarders, offer continuous spectral tunability on brief time scales (see Fig. 10). The Kurios WL1 from Thorlabs is the device employed as baseline LCTF for the ∱ISPEx instrument. This selection comes from a tradeoff among commercially available LCTFs. The following list summarizes the LCTF specs as provided by

the manufacturer: 1) wavelength range is 0.42-0.73 μm; 2) bandwidth (FWHM) is 35 nm at 0.55 μm; 3) polarized transmission is 45 45% at 0.55 μm; 4) Out of band rejection is >2; 5) the minimum incremental step is 1 nm; 6) the tuning precision is ±FWHM/10; 7) the clear optical aperture diameter is 35 mm; 8) the field of vision is ±6°; 9) the switching speed is 50 ms; 10) the uniformity over the clear aperture is ±FWHM/4. 11) The damage threshold on a 0.471 mm spot is 0.8 W/cm^2 at 0.532 μm; 12) The operating temperature range is 0 to 40 degrees Celsius; and 13) The storage temperature range is -15 to 65°C. Although this component is completely compatible with the $\int_{0.4}^{1.0}$ISPEx breadboard, its potential application in the $\int_{0.4}^{5.0}$ISPEx instrument needs to be assessed since it is not space-qualified.

IMG channel objective The light beam is focused on the imager detector by an f/#=7.3, F=257 mm, D=35 mm objective made of 6 spherical lenses arranged in 2 groups after being wavelength-filtered by the LCTF. Table A.1 lists the optical properties of the objective. The target can cover a maximum field of ±1.65° × ±0.8°. Different glasses (CaF2, LAK9G15, K5G20, Suprasil, and Sapphire) were used to make the objective's lenses in order to optimize transmission and reduce chromatic aberration in the 0.42-0.73 μm spectral range. These materials can be used in space applications since they are rad-hardened. Additionally, in order to avoid using optical adhesives, the lenses are not attached in groups but rather separated from one another. To lessen internal reflections and increase transmittance, each lens' surface must be treated with an anti-reflection coating. The first lens' surface, where the LCTF module will be mounted, is at 56.5 mm from the entry pupil of the objective. The detector is located at the same location as the focal point, which is 245 mm from the first lens surface.

IMG channel focal plane The IMG optical design has been optimized for the adoption of a sensor with an active size of 4120×2060 pixels with a pixel pitch of 3.76×3.76 μm. The Sony's APS CMOS sensors models IMX455ALK-K and IMX571, which differ in format size (Full-Frame vs. APS-C) have comparable requirements. The two sensor show slight variations in dark current (being the MX571 model characterized by a smaller value, see specifications listed in Table 4). Both of these models' properties make them ideal to be used as the focal plane for the IMG channel. The IMX571 model is the preferred option for the $\int$ISPEx flying model because of its smaller size and reduced dark current, despite the fact that the two detectors have similar performances. The Sony IMX455ALK-K focal plane included in a commercial camera (QHYCCD QHY600-PH) is utilized in the $\int$ISPEx breadboard model that is tested in the lab. The detector in this camera can be cooled down to -35°C thanks to a two-stage TEC cooler and an antidew thermal control. It can download data at a speed of 2.5 full frames per second thanks to its integrated 1 GByte DDR3 memory and USB3 data interface. The camera's maximum power consumption is 13.8 W at steady state at -20°C and 40 W during cooldown. The QHY600 PRO camera weighs 980 g.

3.4. Visible Spectrometer (SPE-VIS) optical layout

The Coded-Mask Optical Reformatter (CMOR) optically connects the Visible Spectrometer (SPE-VIS) to the OH .The SPE-VIS objective focuses the collimated light beam that has been reflected by the dichroic filter on the circular entrance of the CMOR bundle, where it is reshaped along the spectrometer's equivalent entrance slit to enable the acquisition of the hyperspectral cube using the coded mask technique. The optical configuration of the SPE-VIS spectral channel is provided in the following sections.

Table 4. Specification of the Sony IMX455ALK-K and IMX571 focal planes for the IMG channel. IMX455ALK-K is employed in the breadboard model, IMX571 is the baseline for the flight model.

Image sensor	**SONY IMX455ALK-K**	**SONY IMX571**
Sensor Technology	Full Frame CMOS	APS-C CMOS
Sensor Type	Back Illuminated	Back Illuminated
Pixel Pitch	3.76×3.76 μm	3.76×3.76 μm
Sensor surface window	AR+AR Multi-Coated	AR+AR Multi-Coated
Effective pixels	9576×6388	6284×4210
Effective image area	36×24 mm	23.6×15.8 mm
Full well capacity in ke$^-$ (standard; extended)	51; 80	51; 75
A/D converter	16 bit	16 bit
Full frame rate	2.5 FPS (USB3)	6 FPS (USB3)
Readout Noise in $^-$ (high; low gain)	1.0; 3.7	1.1; 3.5
Dark current in e$^-$/px/s (at -20°C; -10°C)	0.0022; 0.0046	0.0005; 0.001

SPE-VIS objective The SPE-VIS objective is based on a custom lenses design with a f/#1.28, F=44.8 mm, and FOV=±0.25°). The complete specifications of the SPE-VIS objective are in Table A.1. To optimize transmission while minimizing aberrations, the objective design includes seven spherical lenses, three of which are aspherical, manufactured of various materials (CAF2, BK7G18, K5G20, LF5G15, SF8G07). To prevent manufacturing issues with aspherical surfaces using this material, all CAF2 lenses in the design are spherical. At 55 mm in front of the primary lens surface is where the objective entry pupil is situated. An electromechanical shutter is positioned at the exit of the objective to enable the measurement of the dark current of the detector and background contribution of the CMOR and spectrometer's structure when commanded on the close position. The objective focuses the image formed by the afocal telescope on the CMOR's 2D entrance terminal which is located on axis at a distance of 75.5 mm from the first lens surface.

SPE-VIS Coded Mask Optical Reformatter (CMOR) The CMOR adopted for the VIS channel is a typical "Wound Glass Bundle" manufactured by Schott primarily for uses with medical endoscopes. About 4000 optical fibers are arranged in a circular bundle with a 0.45 mm diameter and ≈70 cm length. Each fiber has a diameter of 6.4 μm, and the spectrum transmission is depicted in the left panel of Figure (4). The multimode fibers have a numerical aperture NA=0.39 that is ideal for imaging applications. As a result, each fiber collects optical rays within a cone of semiaperture 23.1°, equivalent to a f/#1.28. Such aperture is comparable to the one of the SPE-VIS objective allowing to maximize the optical throughput while minimizing vignetting. In the right and center panels of Figure 4, respectively, a microscope picture of the 2D entrance fiber bundle terminal and an image of the test bundle ferrula are displayed.

The output terminal (label 13 in Fig. 3) is modified with the intention of keeping all fibers along a straight line corresponding to the geometry of the spectrometer's entry slit. The distance between adjacent fibers is kept constant at 7.52 μm, corresponding to the size of the detector's pixel. Two consecutive fibers can be positioned with a margin of 1.12 μm on average. The 1D output terminal has a width of 6.4 μm (e.g. the diameter of each single fiber) and a total length of 4000×7.52 μm = 3.01 cm. Along the slit direction, the fibers are arranged in casual order. The reworking of the circular terminal of the Schott bundle in linear order, is under responsibility of CNR-IFAC (Istituto di Fisica Applicata "Nello Carrara") in Sesto Fiorentino, Florence, Italy. CNR-IFAC has a history of producing fiber connections with specialized designs for the physical and medical sciences. Due to the intricacy and high

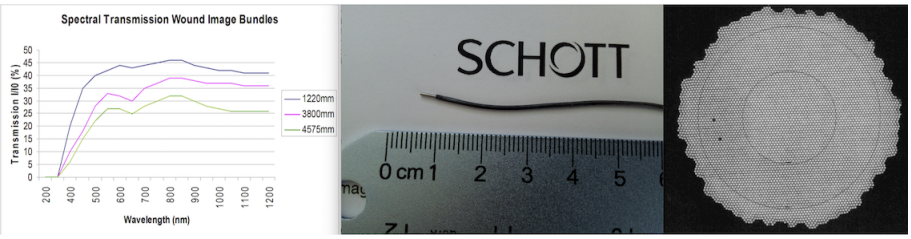

Fig. 4. Left: Transmission curves of Schott "Wound Glass Bundle" with lengths of 1220, 3800 and 4575 mm. Center: Photo of the Schott CMOR bundle 2D entrance terminal. Right: Microscope image of the Schott CMOR bundle 2D entrance terminal. The overall bundle diameter is 0.45 mm and the size of each fiber is 6.4 μm.

accuracy required to post each fiber in conformity with the optical requirements, a two-arm micro-manipulator fitted with a microscope is utilized to capture, position, and glue each individual fiber above the mechanical support. With the intention of facilitating the placement, glueing, and alignment of the fibers, the support's surface has been etched with a ruled V-shaped groove pattern (with periodicity of 7.52 μm) realized through a laser ablation process (direct "writing"). The manufacturing process of the CMOR is still ongoing at the time of writing of this manuscript. The instrument uses the "Coded Mask" approach to reorder the spectrum corresponding to each fiber position inside a hyperspectral data cube by describing the relationship between the location of each fiber *(x,y)* on the entrance 2D terminal and the corresponding position *(n)* on the output 1D terminal. This method allows one to achieve integral-field imaging spectroscopy since it uses a single snapshot to create the spectrally dispersed signal of each spatial fiber. For the IR spectral range, a similar optical arrangement is used, but with different settings (see section 3.5).

SPE-VIS Dyson Spectrometer The SPE-VIS spectrometer is fed with light via the 4000 fibers positioned along the CMOR 1D linear terminal. The input slit of the corresponding spectrometer is therefore equivalent to the linear fibers array. The spectrometer uses a Dyson design employing a convex reflecting grating (33.8 grooves/mm, D=130 mm, marked with label 15 in Fig. 3) to scatter the beam, which is then focussed on the detector (label 16) via a double passing through a three-lens objective (label 14). The optical system, which operates at unitary magnification, is telecentric. All of the lenses are spherical made of fused silica and CaF2. Table 5 includes a list of the grating specs.

Table 5. Specification of the SPE-VIS and IR gratings parameters.

Specification	Value (VIS)	Value (IR)
Spectral Range (μm)	0.4-1.05	0.95-5.0
Grating Type	Concave grating	Convex grating
Radius of curvature (mm)	235.27	166.718
Diameter (mm)	130	70
Grooves density (grooves/mm)	34	59.3
Incident Angle (chief ray axial field) (°)	3.47	52.5
Diffraction order	-1	1

We estiamte an overall SPE-VIS optical transmittance of 38% by assuming typical antireflection coating and grating efficiencies. Optical analysis of the Dyson spectrometer shows that the point spread function is substantially contained inside a nominal 8x8 μm pixel. Over the whole detector area, the optical aberrations are predicted to be <1.02 μm for the keystone and <1.43 μm for the spectral smile. The MTF sampled at Nyquist frequency is > 55% at 1.05 μm on a pixel of 8 μm size, whereas the anticipated polarization, ignoring the grating contribution, is < 3%.

SPE-VIS channel focal plane The primary criteria of the SPE-VIS detector are: 1) a pixel pitch matching the dimension of the optical fibers diameter in the CMOR, and 2) a broad format along the spatial axis sufficient to fill the slit length since the SPE-VIS optical architecture has unitary magnification. The SONY IMX455ALK model, which is the same detector considered for the IMG channel (see Table 4), is the best CMOS detector to match the fISPEx-SPE VIS channel, according to a tradeoff among commercially available detectors. We plan to operate this detector, which has a 3.76 μm pixel pitch, by binning two physical pixels to create an equivalent spatial pixel of 7.52 μm. With fibers of 6.4 μm in diameter, a comparable size may be employed, supposing the 1D terminal is realized as mentioned in section 3.4. Only a portion of the SONY IMX455ALK CMOS detector, or 8000 physical pixels along the spatial (sample) axis and 975 pixels along the spectral (bands) axis, is employed. Binning two pixels in the direction of the slit results in the 4000 spatial samples format. The spectrometer's full spectral range (equal to 650 nm) spans across a distance of 3.666 mm on the detector, resulting in a dispersion of 177.3 nm/mm. As a result, pixels along the spectral axis are binned ×6 , yielding a sampling of 4.0 nm/band over 163 bands. Each VIS-SPE channel acquisition corresponds to an array of 4000 by 163 (samples by bands) pixels with a binning of 2 by 6 (spatial by spectral axis) pixels. By using spectral binning ×4, which results in spectra resolved over 244 bands, it is possible to attain higher spectral sampling (2.7 nm/band). In this instance, each acquisition is determined by 4000×244 pixels (2×4) binning. Fig. 5 depicts a coupling scheme between fibers and pixels. The SONY IMX455ALK CMOS detector's capabilities (dark current and quantum efficiency) are the same as those previously covered in section 3.3. The detector is mounted in thermal contact with the SPE-VIS mechanical structure in order to passively cool it to operative temperature (T< 230 K). The detector will be equipped with a linear variable spectral filter, which is required to exclude higher orders generated by the grating.

3.5. Infrared Spectrometer (SPE-IR) optical layout

The Infrared Spectral channel (SPE-IR), like the SPE-VIS, is optically coupled to the OH by a dedicated IR CMOR. The SPE-IR objective (label 12 in Fig. 3) focuses the collimated light beam transmitted by the dichroic filter (label 9) on the CMOR entrance terminal.

SPE-IR objective The purpose of the SPE-IR objective is to focus the image collected through the telescope above the 2D entrance terminal of the IR CMOR. The four spherical lenses in the f/#=2.5, F=87.5 mm, D=35 mm SPE-IR objective are made of diverse materials (BaF2, Sapphire, and ZnSe) with the goal to optimize transmission while minimizing aberrations. The adopted architecture enables very small lateral color and spots that are smaller than the fiber core. The first lens is placed 55 mm in front of the objective entry pupil. An electromechanical shutter is positioned at the optical beam's exit to enable the measurement of the detector's dark current and the thermal background contribution of the CMOR and spectrometer's construction when the blade is rotated on the closed position.

IR Coded Mask Optical Reformatter The IR CMOR is made by a bundle of 484 multimode fibers in IFG (Indium Fluoride Glass), which Le Verre Fluore (LVF) manufactured using a customized procedure. Each fiber has a core that is 80 μm in diameter and a cladding that is 100 μm in diameter. The fibers have a Numerical Aperture (NA) value of 0.2, which equals f/#=2.5. To prevent vignetting, this aperture corresponds to the one of the IR objective's as specified in the preceding section. The IR channel also employs a coded-mask design, similar to the VIS bundle. A square measuring approximately 2.2 mm by 2.2 mm and housing an array of 22×22 fibers is the bundle entrance terminal. The image focussed by the SPE-IR objective is collected by this terminal. On the output terminal (label 18 in Fig. 3) the 484 fibers are mounted along a line with an optical width of 100 μm, which corresponds to the diameter of a single fiber's cladding, and a length of 48.4 mm. The arrangement of the fibers along the output terminal is arbitrary, and during the calibration process will be characterized how they correlate to their positions on the input terminal (coded mask approach). Fig. 5 depicts the two terminals setup in its entirety.

IR Offner Spectrometer The output terminal of the IR CMOR acts as the equivalent slit of the IR spectrometer which is based on a Offner f/#2.5 design, and it is intended to disperse light across the 1.0-5.0 *mu*m spectral range. The optical beam is angled by a plane mirror (label 19 in Fig. 3) towards a corrective lens (label 20). After passing through the lens the beam is collimated by the Offner primary mirror which is divided in two halves to reduce mass (labels 21a-21b) before reaching the grating (label 22) who reflects the diffracted rays again on the second halve of primary mirror. The dispersed beam is further corrected and focused by a second lens (label 23) on the position where the IR detector (label 24) is mounted. Both corrective lenses are made in Cleartran. The grating is convex-shaped, has a diameter of 70 mm, and a groove density of 59.3 1/mm (see Table 5). The physical dimension of the single IR fiber on the output terminal is preserved along the spatial axis of the detector since the spectrometer has unitary magnification. Based on a preliminary study, it is possible to maximize the grating's efficiency such that it is equal at the two spectral edges (min efficiency 0.18 at 1 and 5 μm). At around 1.7 μm, an efficiency of 0.9 is attained. A multiblazed grating profile can be used to further optimize the performances. The IR spectrometer's aberrations are well-corrected, according to optical analysis: by design, the maximum keystone is 1 μm and the smile is 1.85 μm. At Nyquist frequency and with an assumed pixel pitch of 80 μm, the MTF is >95 % at 0.95 μm and >85 % at 5 μm. The spectrometer's total optical transmission, accounting for grating efficiency, is >0.16, and its polarization sensitivity is $< 3 \div 4\%$ (not including the polarization introduced by the grating).

SPE-IR channel focal plane Although this arrangement is conceptually the same as the one described for the VIS spectrometer, there is a significant variation in the data acquisition modalities between the two spectrometers. The whole portion of the fibers in the VIS channel is totally optically active as a result of the

extremely thin (few nanometers) coating deposited on the wound glass fibers, making it feasible to match the 7.52 μm pixel pitch on the detector with the diameter of the fibers on the CMOR (see Fig. 5). In order to account for the space required to glue the fibers along the output connection, we kept a $\approx$1 μm margin. Fig. 5 shows the diagram illustrating the superposition of the three channels' FOVs and the CMOR configuration of the IR, VIS-NIR, and spectrometers.

A comparable strategy is not practical for the IR channel because the 10 μm thick cladding that surrounds each fiber core does not transmit light (Fig. 5-top panel). Since the core material's refractive index is higher than that of the cladding, light traveling through the core that encounters the cladding's boundary at a smaller angle than the material's typical critical angle will be completely internally reflected back into the core, allowing the light to travel through the fiber from one end to the other. It is not feasible to lower the cladding thickness below 10 μm in the >2.5 μm spectral range given the present production capabilities and material characteristics (internal communication with LVF). The cladding obscuration between successive fibers is equivalent to 20 μm. As the spectrometer's design uses unitary magnification, the spectral information on the detector is gathered along the spatial direction over 80 μm wide blocks separated by 20 μm wide blocks, which correspond to spurious signal coming via consecutive fibers cladding. The Teledyne HAWAII H4RG-10 is one of the available space-qualified IR detectors that might be adapted for use on the fISPEx SPE-IR channel. For the sake of conciseness, just the key parameters required to support the detector's adoption are stated in the following. A complete description of the detector is provided in Loose et al. (1981). The ability to span across a wide slit length and the pixel pitch size commensurable with the optical fibers core size and cladding diameters are the two key criteria guiding this selection. By binning adjacent pixels, the Teledyne HAWAII H4RG-10's 10×10 pixel pitch enables it to match the dimensions of the fiber core and cladding. In order to maintain the signal's purity as it travels through the fibers, a binning of 8 pixels along the spatial axis that corresponds to the fiber's core size (80 μm) must be interspersed with two pixels that correspond to the cladding block's width of 20 μm. Binning 8 pixels allows for the desired sampling along the spectral axis. It takes two side-by-side buttable detectors to cover the complete spatial axis since the detector side is smaller (41 mm) than the comparable slit length, which is 48.4 mm. Due to the unique architecture of the HAWAII H4RG detector, it is feasible to assemble a 8192×4096 focal plane by linking two identical detectors side by side. In a similar setup, the detector gathers the fiber core signal by binning ×8 times along the spatial axis, and then skips the cladding block by interleaving two pixels rows. In accordance with the length of the analogous slit, this approach is repeated 484 times (Fig. 5). The whole SPE-IR spectrum spans 4000 nm across a 4.0 mm width, resulting in a dispersion of 1000 nm/mm. Binning ×8 pixels along the spectral axis results in a sample of 8 nm/band. The spectral axis is sampled by 506 bands following spectral binnng. After binning and removing pixels from cladding blocks, each acquisition of the IR-SPE channel corresponds to an array of 484×506 (samples by bands) equivalent pixels. The signal associated to each equivalent pixel is the sum of the signals collected by 64 physical pixels on the detector. For the future, Teledyne HAWAII 4RG-10 detector may theoretically be replaced with a detector with a larger 20 μm pixel pitch, which would allow the number of binned pixels to be decreased from 8×8 to 4×4, improving readout noise and non-uniformity response. However, the most common manufacturers of IR detectors do not currently provide 20-μm pixel pitch. The ability to employ specialized proximity electronics to control, collect, and digitize the data from the detector is a significant benefit of the Teledyne design. An integrated SIDECAR ASIC circuit handles these tasks. The SIDECAR is an integrated focal plane electronics device that fits on a single chip. A flex cable (separate FPA-ASIC devices) or socks are used to link the ASIC's 36 digi-

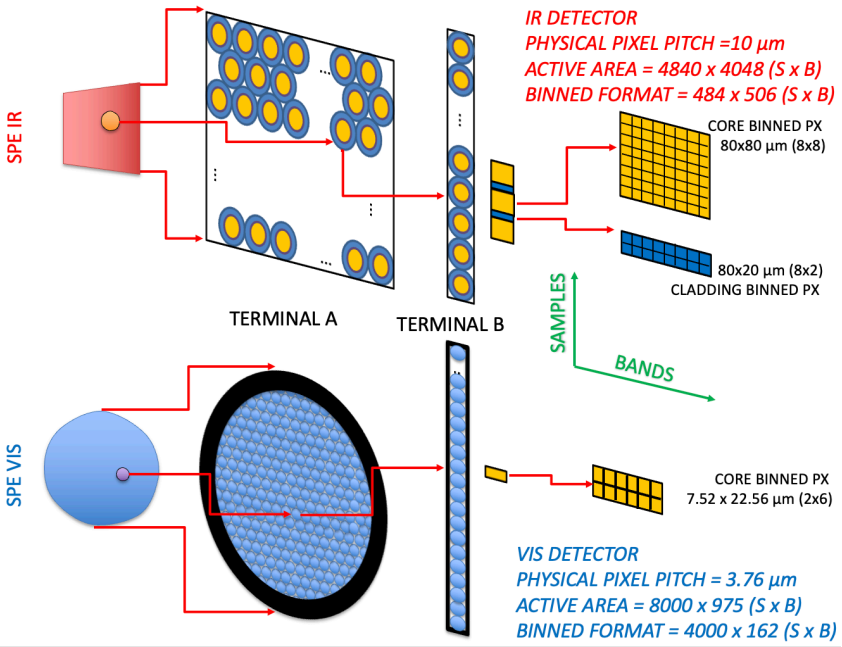

Fig. 5. Top panel: sketch showing the superposition of the IMG, SPE-VIS and SPE-IR field of view, CMORs 2D image to 1D slit terminals and light dispersion across the two corresponding detectors. Bottom panel: arrangement of the fibers within the two CMORs and coupling with detectors' pixels. Input CMOR terminals A for SPE-VIS and SPE-IR are labelled respectively as 14 and 21 in Fig. A.1). Terminals B are the output 1D equivalent slits (16 and 23 in Fig. A.1) placed at the VIS/IR spectrometer entrances. Active areas and binnings are indicated for VIS and IR detectors.

tal processing channels to the detector's output ports (integrated FPA-ASIC units). These channels have the ability to sample the signal at either 16 bit at 500 KHz (slow mode) or at 12 bit at 10MHz (fast mode). In slow and rapid modes, the ASIC uses <300 mW and <1 W of power, respectively. The IR detector uses an external radiator labeled R2 in the block diagram on Fig. A.1 to passively cool it at its operating temperature (T<90 K). A special thermal strap conductively connects the focal plane to the radiator (label TS2). Prior to the focal plane, we plan to introduce a linear variable spectral filter necessary to reduce higher-order grating radiation and out-of-band straylight.

3.6. Main Electronics

The Main Electronics unit (EU, Fig. A.1) is housed in a single mechanical structure containing the following discrete boards

1. Power Converter and Distribution Unit (PCDU), connected to the S/C power interface;
2. CPU and data link with the S/C interface (ME);
3. Proximity Electronics necessary for the readout and digitalization of the IMG detector (PE-IMG);
4. Proximity Electronics necessary for the readout and digitalization of the SPE-VIS detector (PE-VIS);
5. Proximity Electronics necessary for the readout and digitalization of the SPE-IR detector (PE-IR);

6. Auxiliary electronics for the commanding and powering of mechanisms (optional scan mirror, shutters) and internal calibration sources (AUX);
7. Liquid Crystal Tunable Filter Controller (LCTFC).

The on board software will manage the timing of the different operations of the instrument (off, idle, science, calibration, maintenance) through which the instrument is commanded, to acquire data and engineering parameters telemetry, and to format and compress science data.

4. Physical resources and temperature budgets

Three bipods that serve to secure the structure while retaining its stiffness (first mode greater than 130 Hz) and minimize the thermal flux between the spacecraft (assumed at 300 K) and the optical head structure (operational T=110 K) are used to attach the fISPEx OH on the spacecraft interface. To enhance thermal insulation and stiffness, the bipods are made in kevlar with mechanical connections made of titanium. The OH structure's initial mode, which is seen in Fig. 6-left panel, was determined by a modal analysis. A dual-stage flat radiator is mounted on top of the OH structure; the largest one (size=1×1m, orange in Fig. 6-right panel) is utilized to cool the OH structure, including the VIS detector, at T≥110 K while the smaller one (0.5×0.5 m, in magenta) keep the IR detector at T≤90 K.

4.1. Mass Budget

In Table 6, an overview of the fISPEx mass budget that includes a 20% margin is provided. Due to the fact that it will rely on the spacecraft's allotment, the internal harness between OH and EU and any Multi Layer Insulation (MLI) are not included.

Unit	Mass (kg)
Optical Head,	28
Electronics Unit	4.8
Nominal Mass	32.8
Total Mass (20% margin)	39.5

Table 6. Mass budget.

4.2. Physical Dimensions

Table 7 provides a summary of the fISPEx physical dimensions budget. Depending on the findings of the thermal analysis, the passive radiator may be greater than the figures indicated. The mechanical drawing for the fISPEx Optical Head unit, which includes radiators and bipods, is depicted in Fig. 6.

Instrument Unit	Physical dimensions (max values, cm)
Optical Head	$77 \times 56.5 \times 40$
Warm Radiator	100×100
Cold Radiator	50×50
Electronics Unit	$25 \times 30 \times 15$

Table 7. Physical dimensions.

4.3. Power Budget

In Table 8, a tentative fISPEx power budget is provided. The instrument relative response is tested using two internal calibration sources that are tuned for the IMG/SPE-VIS and SPE-IR channels during the internal calibration mode, which has a maximum duration of <5 minutes. Throughout the on-ground testing, cruise, and science stages, this mode will be regularly employed.

4.4. Operational and Survival temperatures

Table 9 details the operational and survival temperatures.

Mode	Power (W)	Note	OH	EB
Idle/Safe/Service Mode	5	DPU on, cover closed	2	3
Science Mode	35	Including shutter operation	5	30
Internal Calibration Mode	40	Including calibration sources	10	30
Annealing/Decontamination Mode	50	If necessary	45	5

Table 8. Power budget (including 20% margin).

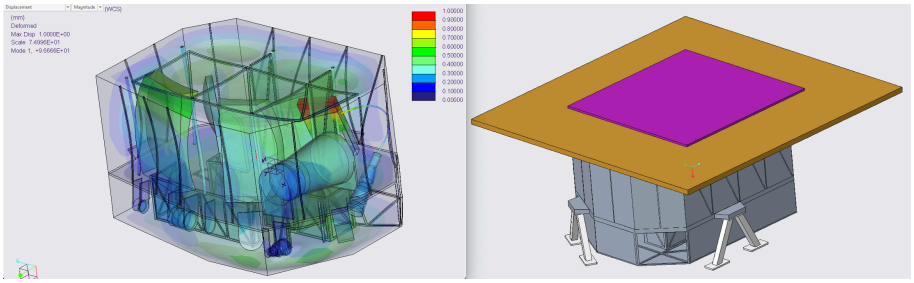

Fig. 6. Left: Optical head first mode simulation. The peak value is 96 Hz. Right: Rendering of the optical head, bipods and radiators (warm radiator is colored in brown, cold radiator in magenta).

Unit	Operative T Min / Nom / Max (K)	Non Operative T Min / Max (K)	Stability (K/hr)
Optical Head	110 / 130 / 150	<100 / >320(*)	±3 (TBC)
IMG detector	243 / 253 / 300	<243 / >320	±3 (TBC)
VIS-NIR detector	243 / 253 / 300	<243 / >320	±3 (TBC)
IR detector	70 / <90 / <100	<70 / >320(*)	±1 (TBC)
Electronics Unit	233 / 293 / 323	<213 / >333	±5 (TBC)

Table 9. Operational and survival temperatures.
(*) excluding annealing and decontamination.

5. The Visibile Imager breadboard

With the aim to verify the performances of the LCTF filter, a breadboard of the $\int$ISPEx Imager has been realized and tested at INAF-IAPS. The breadboard is realized with commercial on-the-shelf components: 1) Thorlabs LCTF model KURIOS WL1; 2) Canon F=300 f/4# telephoto lens; 3) Detector QHYCCD model QHY600-PH. The three optical components are mounted and co-aligned on a linear stage in series. Due to the limited clear aperture of the LCTF, the Canon telephoto lens is operating with a reduced aperture of 35 mm (from 77 mm). An image of the assembled breadboard is shown in Fig. 7. The LCTF filter is commanded through its controller which allow to stabilize temperature and set the filter wavelength. The detector, including the Peltier stage necessary to reach operational temperature $< -20°$C, is commanded through a PC. On a target placed at about 1.5 m of distance, the instrument reaches a spatial sampling of about 20 μm/pixel across a field of view of about 19.2 $\times$ 12.8 cm by adjusting the focus of the telephoto lens. These performances are verified on a standard USAF mask used as a target (Fig. 8).

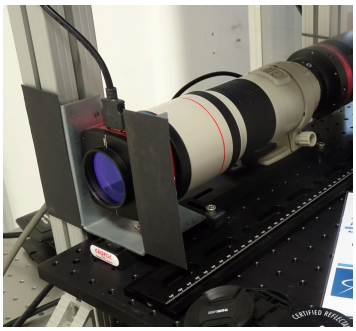

Fig. 7. The Imager breadboard realized in IAPS laboratory with the aim to verify the LCTF performances.

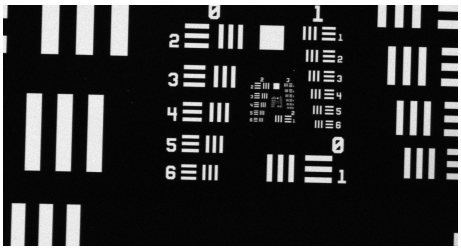

Fig. 8. An image of the reference USAF mask at λ=550 nm taken from 1.5 m distance showing a spatial sampling better than 20 μm/pixel.

6. Calibration of the LCTF

For the spectral characterization of the LCTF, a monochromator is used as a reference light source. The monochromator is placed on the $\int$ISPEx optical bench so that the light emitted from the exit slit is directed on a white Spectralon target (diffuse reflectance $>$ 99% in the 400-1500 nm spectral range) located in front of the Imager camera equipped with the filter. A 150 W QTH lamp powered with a current of 7 Ampere, coupled with the monochromator entrance slit, is used as source of light.

The monochromator is configured with a 300 grooves/mm grating with a 500 mm blaze to improve its efficiency in the visible spectral range. The entrance slit of the monochromator is open to a width of 1000 μm while the exit slit is set at 2000 μm. The main goal of the test is to verify the LCTF transmittance curves, in terms of central wavelength and spectral width response, with respect to the performances declared by the manufacturer (as shown in Fig. 10).

Three sets of measurements have been performed at λ_1 = 480 nm, at λ_2 = 550 nm and at λ_3 = 650 nm. The first set of measurements centered at λ_1 has been made by scanning with the monochromator the range between λ = 440 nm and λ = 520 nm at increments of 5 nm/step. For each step both the signal and the background are acquired. The background is mea-

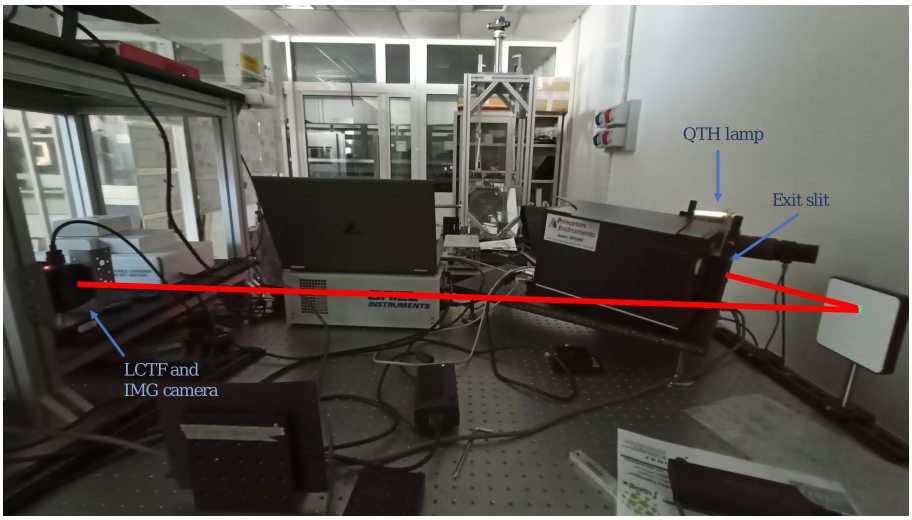

Fig. 9. Sperimental setup. The light beam emitted by the monochromator is diffused by the Spectralon target towards the Imager breadboard imager equipped with the LCTF. The green spot of the monochromatic light at λ=550 nm is visible on the Spectralon. The Imager line of sight is perpendicular to the Spectral surface (emission angle e=0°) while the monochromator beam is incident at an angle i=30°.

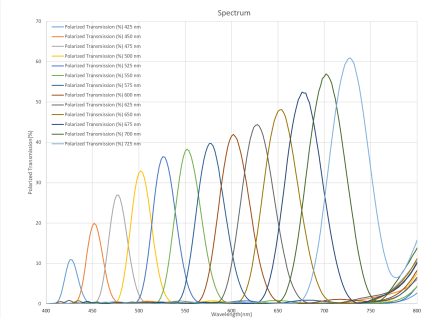

Fig. 10. Thorlabs Kurios WL1 LCTF spectral response curves for light polarized parallel to the filter's transmission axis (from Thorlabs).

sured by shutting off the optical beam at the exit of the monochromator. These acquisitions are made with the same integration times of the spectral measurements. In this configuration the Spectralon target is illuminated only by the very low ambient light in the laboratory. The subtraction of this contribution is important to remove the ambient light and the detector's dark current allowing an optimal retrieval of the signal. The detector's dark current has been minimized by cooling it at -20°C during the measurements. In order to avoid saturation, the exposure time is set near the peak of the signal obtaining a time of 3 s. On each step the acquisitions are subtracted by the collected background. On the resulting images a Region Of Interest (ROI) above the Spectralon is selected and the corresponding average signal is computed together with its standard deviation. The obtained data are normalized with respect to the monochromator's grating spectral efficiency in order to take into account its spectral response and equalize the curve with respect to the maximum. The data points are shown with their error bars derived from the computation of the Signal-to-noise (S/N) ratio: a second ROI is selected on an area of the Spectralon image not illuminated by the monochromator's beam. The resulting average signal of this ROI can be considered a measurement of the noise to be used to compute the S/N ratio by dividing the previously obtained signal by the noise. The error on the measurements is inversely proportional to the S/N being:

$$error(\lambda) = \frac{x(\lambda)}{S/N(\lambda)} \quad (2)$$

Fit at: (nm)	Center λ (nm)	FWHM (nm)	Height (DN)	StDev (nm)
480	477.995	28.459	485.083	12.110
550	545.690	35.307	431.960	15.024
650	643.955	45.798	597.704	19.489

Table 10. Coefficients of the gaussian fits on the measured spectral scans at 480, 550 and 650 nm.

The resulting signal curve, gaussian fit and parameters are shown in Fig. 11.

A similar processing is repeated after setting the LCTF center wavelength at λ = 550, 650 nm. The resulting spectral transmission curves and fits are shown in Fig. 12-13 and summarised in Table 10.

The fitted signals have peak wavelengths λ_1 = 477.995 nm, λ_2 = 545.690 nm and λ_3 = 643.955 nm. Comparing them to the target wavelengths, the obtained error percentages are respectively of 0.419 %, 0.790 % and 0.939 %, indicating that the wavelengths have been measured accurately. The obtained differences might be partly related to the LCTF tuning accuracy. As declared by the manufacturer, this is equal to $\pm FWHM/10$. The differences between the measured spectral response of the filter and the declared wavelengths from the manufacturer are: $\Delta\lambda_1$= 2.005 nm, $\Delta\lambda_2$ = 4.310 nm and $\Delta\lambda_3$ = 6.045 nm. The error affecting the measurement at λ = 480 nm falls within the expected error, while the other two exceed it slightly. The filter bandwidths declared by the manufacturer are 22, 30 and 42 nm at 480, 550 and 650 nm, respectively. From the measurements we have obtained: 28, 35 and 46 nm, resulting in a maximum difference $<$ 5 nm. It should also be taken into consideration the possibility of systematic errors in the instrument and in the setup (in particular in the monochromator) as well as random errors, due to not having repeated measures, which may have affected these results. Overall, the results obtained with the fISPEx breadboard seem to show a bias of the LCTF spectral response of a few nanometers towards shorter wavelengths, which becomes more evident for longer wavelengths while the spectral width appears larger than the declared one by at least 5 nm. However, all these effects can be easily compensated during the calibration of the instrument. Noteworthily, this setup has been used to acquire hyperspectral data of Ryugu grains (Ferrari et al. 2023) as well as several meteorite samples.

7. Conclusions

The fISPEx concept has been designed starting from the lessons learned in INAF-IAPS from more than 25 years of technical and scientific experiences in the field of imaging spectrometers and cameras for space applications. Within the framework of this project which has been fully financed through a competitive call issued by the Italian Space Agency (ASI) and the italian National Institute for Astrophysics (INAF), a very positive collaboration among INAF, Politecnico of Milan, CNR-IFAC and Leonardo has been established and new new expertise in the field of photonic devices (LCTF, CMOR) has been acquired. The team has approached new ways on how to optimize the scientific return from VIS-IR imaging spectrometers and color cameras through data fusion and integration of science/operation teams.

Thanks to its intrinsic modularity, it is possible to adapt the fISPEx design to different optical architectures (telescopes and microscopes), platforms (orbiters, landers, rovers) and missions scenarios (planetary or Earth observation; laboratory and field analyses). A complete phase-A study for the flight instrument has been redacted and delivered as the main product of the study. This material and additional one not published here is available to ASI for consideration in future proposals and flight opportunities.

One of the purposes of the fISPEx study was to explore new solutions to perform integral field spectroscopy and to design an integrated instrument which could be adapted for a generic Near-Earth Asteroid mission. Given

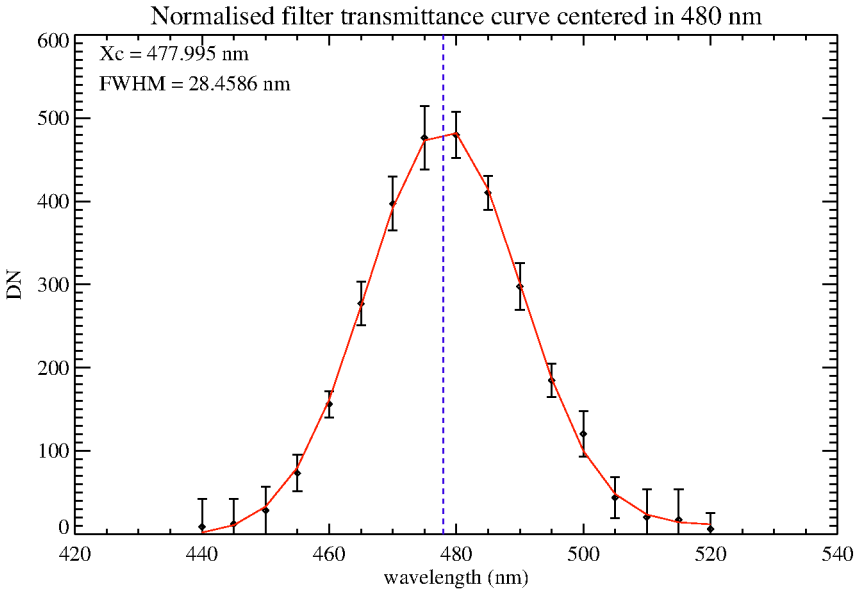

Fig. 11. Measurements (black points) and gaussian fit (red curve) of the LCTF transmittance centered at 480 nm. The error bars show the error derived from S/N measurement and are amplified by a factor of 5 for sake of visibility. The signal is normalized for the monochromator's spectral response.

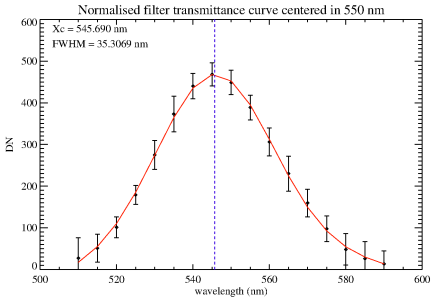

Fig. 12. The same as Fig. 11 but for λ=550 nm.

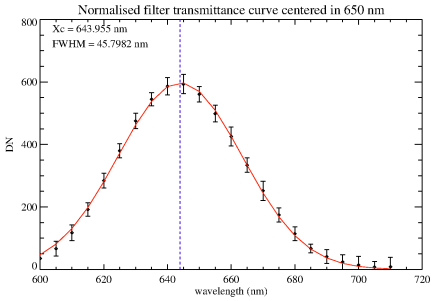

Fig. 13. The same as Fig. 11 but for λ=650 nm.

the limited fundings and schedule of the program, the ƒISPEx team was forced to adopt an optical configuration based on commercial (on the shelf) photonic devices like LCTF, CMOR and detectors. As a result of these constraints, despite the efforts to optimize the design, the instrument operates with different FOV and IFOV across its three optical channels (see Table A.1). Another limitation is the relatively small size and different shape of the two spectrometers' FOVs. These issues must be carefully considered when planning any future observation scenario because they will impact on the spacecraft orbital and attitude profiles.

With the rapid progresses occurring in photonic research, we foresee that it will be possible in the near future to further improve the ƒISPEx design. In fact, 1) new LCTF with wider spectral range and/or smaller bandpass will extend the Imager capabilities; 2) IR fibers with smaller diameters will permit to build

denser CMOR assemblies resulting in a spectrometer's design offering a smaller IFOV and larger FOV; 3) the manufacturing of custom-design CMOR assemblies will improve the matching with optical elements and detectors.

Despite the difficulties occurred during the COVID pandemic, a representative breadboard unit for the fISPEx IMG channel has been realized and tested in IAPS lab. The high performances of the breadboard have been exploited to collect scientific data on various mineral samples and several ongoing science programs have shown interest in using it to perform hyperspectral imaging at high resolution of samples. The realization of the VIS CMOR is still ongoing due to the complex manufacturing process of the component for which further developments would be needed. The fISPEx instrument's concept has been presented in both national (Filacchione et al. 2022a) and international conferences (Filacchione et al. 2022b) where it has been discussed with the community.

Acknowledgements. We gratefully acknowledge the financial contribution for the development of scientific instrumentation from the Agreement ASI (Italian Space Agency) - INAF (Italian National Institute for Astrophysics) n. 2018-16-HH.0 "Attività di Studio per la comunità scientifica nazionale: Sole, Sistema Solare ed Esopianeti". GF thanks the technical support received from dr. Stefan Weiser and dr. Michael Dargie (Schott, Germany-USA), and dr. Laurine Bodin and dr. Samuel Poulain (Le Verre Fluoré, France). We grateful thank INAF-IAPS colleagues Stefania Stefani, Simone de Angelis, Eliana La Francesca and Marco Ferrari for technical support during the fISPEx breadboard integration and measurements. This research has used NASA's Astrophysics Data System.

Appendix A: Block Diagram and Instrument Specifications

The instrument is made by four subunits: the *Optical Head (OH)*, the VIS Spectrometer (SPE-VIS), the IR Spectrometer (SPE-IR) and the *Electronics Unit (EU)*. The instrument block diagram, including subsystems, electrical and thermal harness, is shown in Fig. A.1. A summary of the optical specifications is given in Table A.1.

Authors

F. Cosi[5], A. Galiano[1], M. Zambelli[1], A. Boccaccini[1], F. Nuccilli[1]

Affiliations

[6] CNR-IFAC, Istituto di Fisica Applicata Nello Carrara, Via Madonna del Piano, 10 50019, Sesto Fiorentino (FI), Italy

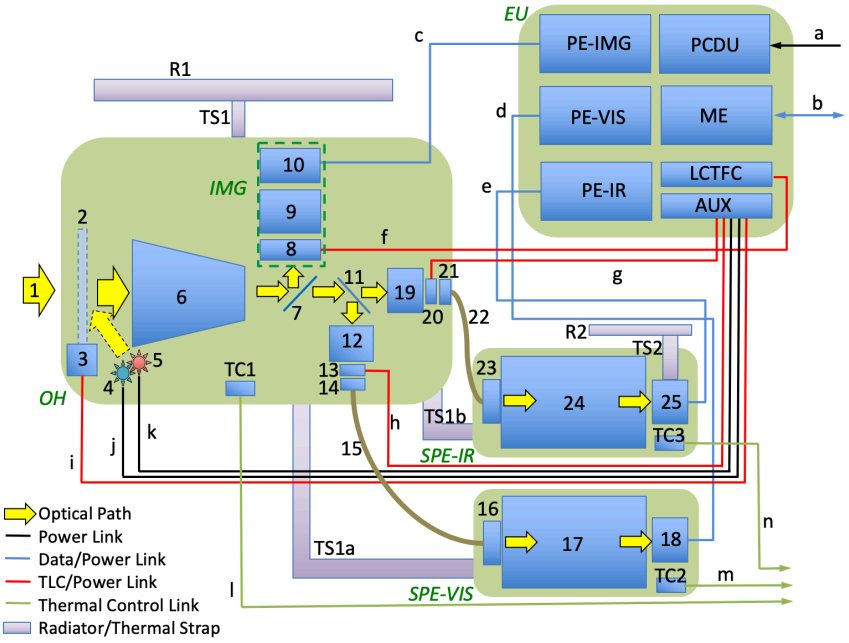

Fig. A.1. Instrument block diagram. Units: *OH* Optical Head, including the Imager *(IMG)* channel; *SPE-VIS* Visible channel spectrometer; *SPE-IR* Infrared channel spectrometer; *EU* Electronics Unit. Subsystems: *1)* Input optical beam (boresight); *2)* Telescope entrance cover, including calibration target on the internal wall; *3)* Cover movement mechanism and motor; *4)* Internal calibration unit VIS lamp; *5)* Internal calibration unit IR emitter; *6)* Three mirror afocal telecope; *7)* Beam splitter (50-50); *8)* LVTF; *9)* IMG objective; *10)* IMG focal plane; *11)* Dichroic filter; *12)* SPE-VIS objective; *13)* SPE-VIS shutter mechanism and motor; *14)* SPE-VIS CMOR 2D input terminal; *15)* SPE-VIS CMOR bundle; *16)* SPE-VIS CMOR 1D output terminal; *17)* SPE-VIS Dyson spectrometer; *18)* SPE-VIS detector; *19)* SPE-IR objective; *20)* SPE-IR shutter mechanism and motor; *21)* SPE-IR CMOR 2D input terminal; *22)* SPE-IR CMOR bundle; *23)* SPE-IR CMOR 1D output terminal; *24)* SPE-IR Offner spectrometer; *25)* SPE-IR detector; *R1)* Passive radiator for OH SPE-VIS and SPE-IR; *TS1)* thermal strap from R1 to OH; *TS1a)* thermal connection between OH and SPE-VIS; *TS1b)* thermal connection between OH and SPE-IR; *R2)* Passive radiator for IR detector; *TS2)* thermal strap from R2 to SPE-IR detector; *PE-IMG)* Proximity Electronics for IMG channel; *PE-VIS)* Proximity Electronics for SPE-VIS channel; *PE-IR)* Proximity Electronics for SPE-IR channel; *PCDU)* Power Conditioning and Distribution Unit; *ME)* Main Electronics; *LCTFC)* LCTF Controller; *AUX)* Auxiliary Board; *TC1)* OH thermal control; *TC2)* SPE-VIS thermal control; *TC3)* SPE-IR thermal control. Harness: *a)* Power link to S/C; *b)* TLC/Data link to S/C; *c)* PE-IMG to IMG detector link; *d)* PE-VIS to SPE-VIS detector link; *e)* PE-IR to SPE-IR detector link; *f)* LCTFC to LCTF link; *g)* AUX to SPE-IR shutter motor link; *h)* AUX to SPE-VIS shutter motor link; *i)* AUX to cover motor; *j)* AUX to internal calibration unit VIS lamp; *k)* AUX to internal calibration unit IR emitter; *l)* TC1 to S/C bus; *m)* TC2 to S/C bus; *n)* TC3 to S/C bus. Lines functionalities are color coded in black for power links, blue for data/power links, red for TLC/power links, green for thermal control links. Optical paths are shown in yellow. Radiators and thermal straps in violet.

Table A.1. Instrument optical specifications.

Telescope	Three mirrors afocal	unobstructed
	Entrance Pupil diameter	84 mm
	Exit Pupil diameter	35 mm
	Beam reduction factor	2.4X
	Field of View	$\pm 0.6875^\circ \times \pm 0.33^\circ$ around boresight
Imager	LCTF spectral range, bandwidth	0.42-0.73 μm, 35 nm at 0.55 μm
	Objective aperture Ø, F, f/#	35 mm, 257 mm, 7.3
	IFOV	14 μrad
	FOV	$3.3^\circ \times 1.6^\circ$ (rectangular)
	Detector type, model	APS, Sony IMX571
	Detector format, pixel pitch	6280×4210 px, 3.76 μm
	Image size, A/D	4120×2060 px, 16 bit
	Spatial resolution from 10 km distance	0.14 m/px
	Spatial coverage from 10 km distance	588×294 m (rectangular image)
SPE-VIS	Objective aperture Ø, F, f/#	35 mm, 44.8 mm, 1.28
	CMOR bundle input terminal	circular, Ø=0.45 mm
	CMOR bundle output terminal	linear, 6.4 μm × 3.01 mm
	Number of fibers in CMOR bundle	≈4000
	CMOR fiber diameter	6.4 μm
	CMOR fiber n.a.	0.39
	IFOV	100 μrad
	FOV	0.4° (circular)
	Detector type, model	APS, Sony IMX455
	Detector format, pixel pitch	9576×6388, 3.76 μm
	Frame size, binning, A/D	8000×972, 2×6 (or 2×4), 16
	Spectral range, dispersion	0.4-1.05 μm, 177.3 nm/mm
	Spectral sampling	4.0 or 2.66 nm/band
	Number of spectral bands	163 or 244
	Number of spatial samples	≈4000
	Spatial resolution from 10 km distance	1 m/pixel
	Spatial coverage from 10 km distance	70 m (circular image)
SPE-IR	Objective aperture Ø, F, f/#	35 mm, 87.5 mm, 2.5
	CMOR bundle input terminal	square, 2.2 × 2.2 mm
	CMOR bundle output terminal	linear, 80(+20) μm × 48.4 mm
	Number of fibers in CMOR bundle	22 × 22 = 484
	CMOR fiber diameter	80 μm (core) + 20 μm (cladding)
	CMOR fiber n.a.	0.2
	IFOV	225 μrad
	FOV	$0.28^\circ \times 0.28^\circ$ (square)
	Detector type, model	HgCdTe, Teledyne HAWAII H4RG-10 (buttable x2)
	Detector format, pixel pitch	8096×4048 px, 10 μm
	Frame size, binning, A/D	484×506 px, 8 × 8, 2 rows interleaved, 16
	Spectral range, dispersion	0.95-5.0 μm, 1 μm/mm
	Spectral sampling	8 nm/band
	Number of spectral bands	506
	Number of spatial samples	484
	Spatial resolution from 10 km distance	2.25 m/pixel
	Spatial coverage from 10 km distance	49.5 × 49.5 m (square image)

References

Ferrari, M. et al., 2023, XVIII Congresso Nazionale di Scienze Planetarie, Perugia, 6-10 February, 2023, abstract 1083.

Filacchione, G. et al., 2022a, XVII Congresso Nazionale di Scienze Planetarie, Naples, 20-24 June, 2022.

Filacchione, G. et al., 2022b, Proceedings of the SPIE, Volume 12188, id. 1218809, 19 pp.

Gaffey, M. J. and McCord, T. B., 1979, Asteroids (A80-24551 08-91), 688–723, Tucson, Ariz., University of Arizona Press.

Hagen, N. and Kudenov, M. W., 2013, Optical Engineering, 52, 090901.

King, T. V. V., Clark, R. N., Calvin, W. M., Sherman, D. M., and Brown, R. H., 1992, Science 255, 1551–1553.

Lebofsky, L. A., 1978, MNRAS, 182, 17P–21P.

Lebofsky, L. A., Astronomical Journal 85, 573–585.

Lebofsky, L. A., Feierberg, M. A., Tokunaga, A. T., Larson, H. P., and Johnson, J. R., 1981, Icarus 48, 453–459.

Loose, M., Beletic, J., Garnett, J., and Xu, M., 2007, in Focal Plane Arrays for Space Telescopes III, Grycewicz, T. J., Marshall, C. J., and Warren, P. G., eds., Society of Photo-Optical Instrumentation Engineers (SPIE) Conference Series 6690, 66900C.

Vilas, F. and Gaffey, M. J., 1989, Science, 246, 790–792.

Vilas, F., Hatch, E. C., Larson, S. M., Sawyer, S. R., and Gaffey, M. J., 1993, Icarus 102, 225–231.

Vilas, F., Jarvis, K. S., Gaffey, M. J., 1994, Icarus 109, 274–283.